

# Magnetic Aggregation I: Aggregation Dynamics and Numerical Modelling

Carsten Dominik

Sterrenkundig Instituut “Anton Pannekoek”

Universiteit van Amsterdam

Kruislaan 403, NL-1089 SJ Amsterdam/The Netherlands

Email: dominik@science.uva.nl

Henrik Nübold

Institut für Geophysik und Meteorologie

Technische Universität Braunschweig

Mendelssohnstr. 3, D-38106 Braunschweig/Germany

Email: h.nuebold@tu-bs.de

October 27, 2018

number of manuscript pages: **40**  
including **0** tables and **5** figures

**RUNNING HEAD: Magnetic Aggregation**

**KEYWORDS: ORIGIN of the SOLAR SYSTEM, MAGNETIC FIELDS,  
COLLISIONAL PHYSICS, COMPUTER TECHNIQUES, METE-  
ORITES**

Please send editorial correspondence and proofs to:

Carsten Dominik  
Sterrenkundig Instituut “Anton Pannekoek”  
Universiteit van Amsterdam  
Kruislaan 403  
NL-1089 SJ Amsterdam  
The Netherlands  
Tel. +31 20 5257477  
Fax +31 20 5257484  
Email [dominik@science.uva.nl](mailto:dominik@science.uva.nl)

## Abstract

Focussing on preplanetary grains growth, we discuss the properties of dust aggregation driven by magnetic dipole forces. While there is no direct evidence for the existence of magnetic grains present in the solar nebula, there are reasons to assume they may have been present. We derive analytical expressions for the cross-section of two interacting dipoles. The effective cross section depends upon the strength of the magnetic dipoles and the initial velocities. For typical conditions the magnetic cross section is between 2 and 3 orders of magnitude larger than the geometric cross section. We study the growth dynamics of magnetic grains and find that the mass of the aggregates should increase with time like  $t^{3.2}$  whereas Brownian motion growth behaves like  $t^2$ . A numerical tool is introduced which can be used to model dust aggregation in great detail, including the treatment of contact forces, aggregate restructuring processes and long-range forces. This tool is used to simulate collisions between magnetic grains or clusters and to validate the analytical cross-sections. The numerically derived cross section is in excellent agreement with the analytical expression. The numerical tool is also used to demonstrate that structural changes in the aggregates during collisions can be significant.

## 1 Introduction

Coagulation of dust grains is generally believed to be the mechanism by which growth of particles in the early solar nebula proceeds from sub-micron grains all the way up to planetesimals (WEIDENSCHILLING AND CUZZI, 1993; BECKWITH *et al.*, 2000). However, many questions remain about the detailed way in which coagulation proceeds, in particular during the initial phase when the particles are still very small and dynamically well coupled to the gas. If the particles are very strongly coupled to the gas, collisions have to rely on the relative velocities induced by Brownian motion (KEMPF *et al.*, 1999). While these slow collisions are certain to result in almost perfect sticking between the grains (CHOKSHI *et al.*, 1993; POPPE *et al.*, 2000), it turns out that they may be too slow to produce the necessary dust growth in the limited time frame available (KEMPF *et al.*, 1999). First of all, the low relative velocities severely limit the number of collisions taking place. As a second complication, the energies involved in the collisions are insufficient to change the structure of the aggregates (DOMINIK AND TIELENS, 1997; BLUM AND WURM, 2000).

Simple hit-and-stick growth in a cluster-cluster aggregation process leads to extremely fluffy aggregates with low fractal dimensions (MEAKIN, 1991; KEMPF *et al.*, 1999). KEMPF *et al.* showed that the Brownian motion leads to fractal dimensions  $D < 2$  for which significant changes in the cross-section-to-mass ratio can only be expected for very large particles. The friction time, i.e. the time in which a particle adapts its velocity to the surrounding gas, changes in a Brownian growth process only as  $r^{1/5}$  with the particle radius. Furthermore, KEMPF *et al.* neglected the rotation of the aggregating particles which will lead to even lower fractal dimensions of the collision product (BLUM *et al.*, 2000). Since the aerodynamic behavior of particles is governed by the friction time (WEIDENSCHILLING, 1977), the aerodynamic properties of large fluffy aggregates and of small grains are almost identical. This poses a serious problem for the coagulation process which must accelerate eventually, in order to fulfill the time constraints given.

Possible ways to accelerate growth have been discussed in the literature, in particular grain settling and radial drift (e.g. WEIDENSCHILLING, 1980), or differential coupling to turbulent eddies of different sizes (WEIDENSCHILLING, 1984; MIZUNO *et al.*, 1988; MARKIEWICZ *et al.*, 1991). Furthermore, aerodynamic concentration is considered as a mechanism to increase densities locally for enhanced coagulation (CUZZI *et al.*, 2001; KLAHR AND HENNING, 1997). However, most of these processes rely on a diversity in the aerodynamic properties of particles: Settling or radially drifting grains will only induce enhanced collision rates if not all grains settle or drift at the same rates. Turbulent eddies will only enhance collision rates if different grains couple to different eddy scales. WEIDENSCHILLING (1997) reports that starting from  $10^{-4}$  cm grains, a high central density of settled dust can still be achieved even if the fractal structure of the grains is taken into account.

Coagulation may proceed on quite different paths if the basic mechanism of coagulation is different from what is normally assumed. An interesting idea was put forward by NUTH *et al.* (1994) and NUTH AND WILKINSON (1995) who studied aggregation of magnetic grains in laboratory experiments. They found that this accretion process proceeds rapidly forming large networks of linear aggregates. NUTH *et al.* suggested that such networks may be important for grain aggregation in the solar nebula. One way in which this mechanism could change the course of aggregation is to turn a cluster-cluster aggregation into a particle-cluster aggregation process. If the networks of magnetic grains can form quickly enough, they may eventually provide a large fraction of the available collisional cross-section in the nebula. The main

aggregation process for non-magnetic grains would then be the collision of a grain with such a network. This mechanism would be physically similar to a cluster-particle aggregation process which produces aggregates with fractal dimension  $D_f = 3$  (BALL AND WITTEN, 1984), leading to more compact structures quickly.

In this article, we will present the foundations for a comprehensive investigation of magnetic dust aggregation from a theoretical and an experimental point of view. We start by reviewing the evidence for magnetic grains in the solar nebula. We will then focus on the physical implications of dipolar interaction between individual dust grains, i.e. enhanced collisional cross sections and accelerated aggregation dynamics. We also present a new numerical tool we devised for the investigation of dust aggregation including a detailed treatment of grain-grain interaction through mechanical contacts, and dipolar (magnetic) forces. We carried out numerical simulations of 2-body collisions with magnetic grains in order to test the code and compare the results with the analytically derived cross sections. Two subsequent papers will communicate our experimental and numerical work of magnetic grain growth on the basis of the material presented here.

## 2 Magnetic dust in the solar nebula

If magnetic interaction is to change the dust aggregation scenario, we have to assume the existence of a nebular dust component carrying remanent magnetization (NUTH *et al.*, 1994; NÜBOLD AND GLASSMEIER, 1999, 2000). The following paragraphs present evidence as to the extent this assumption seems to be justified.

**Formation of chondrules** Many of the small number of pieces that have been found to complete the puzzle of solar nebular physics come from the study of meteorites. KERRIDGE AND MATTHEWS (1988) and KERRIDGE (1993) provide a comprehensive overview of this subject.

An important result from the study of meteoritic material is the occurrence of chondrules, i.e. small spherical inclusions which are embedded in a presumably more primitive matrix. Despite a large number of different hypotheses (BOSS, 1996) as to the origin of chondrules, the consequences of the necessary melting process have been studied intensively. Chondrules are formed when a physical process in the solar nebula melts silicate dust

aggregates followed by rapid cooling of the molten material which congeals as spherical droplets (GIBBARD *et al.*, 1997). Nebula lightning, shock fronts, and friction have been discussed as possible energy sources. The heating process itself has been repeatedly investigated both theoretically and experimentally (LEVY, 1988; GROSSMAN *et al.*, 1988). The heated dust aggregates of possibly interstellar composition undergo internal reduction-oxidation reactions, which result in an evaporative loss of metallic iron from the melt (NUTH, 1989). The iron vapor then condenses into sub-micron-sized dust grains. Depending on the grain size these grains can have different magnetic properties (NUTH *et al.*, 1994; WITHEY AND NUTH, 1999). Very small grains below 20 nm are superparamagnetic, large grains  $> 80$  nm show multidomain behavior. Intermediate sizes, in particular grains between 40 and 60 nm are single domain grains which spontaneously become magnetic dipoles. In a more general way, melting events in the solar nebula will always produce magnetic minerals such as magnetite (RIETMEIJER *et al.*, 1999).

Chondrules themselves originate from already existing aggregates, so the iron grains produced by this process will not have been present very early on in order to start the aggregation process. However, similar melting events must have been a frequent phenomenon in the early solar system. The assumption of an important population of magnetic iron dust appears plausible on these grounds.

**The paleomagnetic record in meteorites** As summarized by SUGIURA AND STRANGWAY (1988), many meteorites exhibit natural remanent magnetization (NRM). The carriers of the NRM are magnetic minerals and metals such as iron-nickel (Fe-Ni: kamacite, taenite), pyrrhotite ( $\text{Fe}_{1-x}\text{S}$ ), and magnetite ( $\text{Fe}_3\text{O}_4$ ; JÄCKEL, personal communication). A possible source for the NRM in meteorites are strong magnetic fields that are assumed to have existed in the solar nebula, magnetizing the dust as it cooled through the Curie point.

It is usually assumed that the NRM in meteoritic material was acquired *after* the formation of the meteorite parent body. However, some meteorites show evidence of heterogeneous magnetization, which could be a hint of magnetization that existed before the dust was incorporated into the meteorite parent body. The magnetization of isolated grains is certainly more easily explained than the magnetization of macroscopic objects, for the latter would require very stable geometric conditions, i.e., a fixed orientation of the ob-

ject that is to be magnetized relative to the magnetizing field. In any case, the paleomagnetic record in meteorites also points toward the existence of a magnetized dust population in the solar nebula.

**Cometary dust** Cometary nuclei are widely supposed to contain the original building material of our solar system in almost pristine form. The great effort which is put into prestigious and adventurous space missions like Rosetta, Stardust, and Deep Space 4/Champollion is a measure of the importance attributed to the analysis of cometary matter.

During the Giotto and Vega missions to comet p/Halley in 1986, mass spectrography of cometary dust grains impacting the spacecraft gave some insight as to the chemical composition of cometary dust. SCHULZE *et al.* (1997) summarized the results of these measurements. Accordingly, Halley's dust is composed mainly of magnesium-rich silicates, but there is an important fraction ( $\geq 10\%$ ) of potentially magnetic minerals and metals similar to those which have been identified in meteorites, i.e. kamacite (nickel-iron), pyrrhotite ( $\text{Fe}_{1-x}\text{S}$ ), and magnetite ( $\text{Fe}_3\text{O}_4$ ).

Some interplanetary dust particles (IDPs) appear to originate from comets (BROWNLIE, 1985). Up to now, no measurements of the magnetic properties of IDPs have been obtained (Bradley, priv. comm.). The presence or absence of aggregates of magnetic grains in cometary IDP would be a direct way to determine if a large population of magnetic grains in the outer solar nebula.

**Asteroids** On its way to the Jovian system, the Galileo spacecraft investigated the asteroids Ida and Gaspra. The magnetic field measurements in the vicinity of the two bodies show significant changes in the solar wind magnetic field as it encounters the asteroids. The magnetic signatures have been interpreted in terms of a remanent magnetization of the two asteroids by KIVELSON *et al.* (1993). The same holds for the encounter of the Deep Space 1 (DS1) spacecraft with the asteroid Braille in 1999 (RICHTER, 2001).

Since asteroids – which should have sizes similar to planetesimals during solar system formation – are much too small to sustain a dynamo, their magnetization could be the trace of primordial magnetic fields or the result of the accretion of previously magnetized material.

**Dust around young stars** ISO observations of young nearby stars have been used to derive the dust properties in the disk around stars close to

the main sequence. Unfortunately, most T Tauri stars are too faint for this, but their higher-mass counterparts, the Herbig AeBe stars, have proved to be excellent targets for such a study WATERS AND WAELEKENS (1998). In several of these stars, the signatures of crystalline silicates have been found (e.g. MALFAIT *et al.*, 1998; BOUWMAN *et al.*, 2000) which are very likely formed by thermal annealing (BOUWMAN *et al.*, 2001). These silicates are *magnesium-rich*, which may leave the iron free to form metallic iron and other potentially magnetic grains.

### 3 The influence of magnetic interaction on the dust aggregation process

In this article we focus on magnetic forces as the only long-range force. Electrostatic interactions between charged grains could be another source of such long-range interactions between dust particles. Their effect on dust coagulation in a nebular context has been investigated both theoretically (HORANYI AND GOERTZ, 1990; OSSENKOPF, 1993) and experimentally (MARSHALL AND CUZZI, 2001). Since the solar nebula is generally considered as optically thick at least in its central regions, photoelectric charging can be ruled out when discussing possible charging mechanisms for dust grains. Triboelectric charging would be due to collisions which usually lead to direct sticking within the range of relative velocities considered here, even if van der Waals interactions are the only attracting force. Therefore, electrostatic interactions are probably of importance only for larger grains (MARSHALL AND CUZZI, 2001).

In the absence of other long-range forces, random thermal agitation is the sole competitor for magnetic interaction. The relative importance of these two effects is generally given by a dimensionless parameter  $\lambda$  defined by:

$$\lambda = \frac{\mu^2 \mu_0}{4\pi d^3 k_B T}, \quad (1)$$

where  $\mu$  is the magnetic moment of the particles,  $\mu_0$  is the magnetic field constant and  $k_B$  is the Boltzman constant. The parameter  $d$  in Eq. 1 defines a certain characteristic interaction distance which is usually taken to be equal to the particle diameter,  $d = 2R$ , or to the sum of the particle radii,  $d = R_i + R_j$ , if we are dealing with multi-disperse grains. For single-domain



particles, which are typically micron-sized or smaller,  $\lambda$  can take on values of the order of  $10^5$  at  $T = 100$  K. In these cases, the aggregation process will not be diffusive but is dominated by magnetic forces. Furthermore, magnetic aggregates should be stable against destructive thermal influences.

According to statistical mechanics, dust particles should acquire a thermal rotational energy  $U_{\text{rot}} = k_B T/2$ , which amounts to very high angular velocities for micron-sized particles. In order to have magnetic interaction overcome this thermal spin-up, the particle-particle interaction energy must be at least of the same order of magnitude. NÜBOLD AND GLASSMEIER (2000) have shown that this happens inside an interaction radius given by:

$$\begin{aligned} R_m &= \left( \frac{2\mu_0}{\pi k_B T} \mu^2 \right)^{1/3} \\ &= 2d\lambda^{1/3}, \end{aligned} \tag{2}$$

which is about 10 to 100 times larger than the actual particle radius for strongly magnetized grains. It is on these length scales that magnetized dust particles “see” each other and interact. In the following sections we will examine some of the consequences in more detail.

### 3.1 Collisional cross section

Grain-grain collisions and sticking in the dilute nebular gas result from relative motion, e.g. due to a thermal distribution of grain velocities. Owing to the minute geometric dimensions of the dust particles, the collision probability is usually very low. Long-ranged forces, e.g. magnetic forces between magnetized grains, lead to an enhancement of collisional cross sections.

Usually, the collisional cross section of a (spherical) particle is simply given by its geometric projection area, i.e.

$$\sigma = \pi R^2, \tag{3}$$

where  $R$  denotes the particle radius. For two colliding particles we have:

$$\tilde{\sigma} = 4 \cdot \pi (R_i + R_j)^2. \tag{4}$$

The collision probability in dust aggregation processes depends directly on the particle cross section: the bigger  $\sigma$ , the shorter the mean free time  $\bar{\tau} \sim 1/\sigma$  between subsequent particle collisions.

NÜBOLD AND GLASSMEIER (2000) investigated this effect for nanometer-sized iron grains numerically, based on the experimental results obtained by NUTH *et al.* (1994). From scattering simulations with spherical iron particles with a diameter of 20 nanometers moving at thermal velocity,  $\sqrt{k_B T/m}$ , it was shown that:

$$\frac{\sigma_m}{\sigma}(v_\infty = v_{th}) \approx 900 . \quad (5)$$

Since the collision frequency depends on the cross section, an enhancement as given by Eq. 5 will cut aggregation time scales by almost three orders of magnitude. From Eq. 2 we see that the cross section may be of the same order as the magnetic interaction radius.

In the calculations leading to Eq. 5 we implicitly assume that magnetized grains are always aligned with the ambient magnetic field, e.g. an external field or the field created by other magnetized dust particles. While this should be the case in terrestrial experiments due to high surrounding gas densities, it is not obvious that instantaneous relaxation of dipoles should occur in very dilute media such as the solar nebula. We will now relax this assumption.

When a magnetic dipole  $\boldsymbol{\mu}$  interacts with another magnetic dipole  $\boldsymbol{\mu}'$  over a distance  $r$ , according to JACKSON (1975) the interaction energy  $U$  can be calculated from

$$U_m = \frac{\mu_0}{4\pi} \cdot \left[ \frac{\boldsymbol{\mu} \cdot \boldsymbol{\mu}'}{r^3} - 3 \frac{(\boldsymbol{\mu} \cdot \mathbf{r})(\boldsymbol{\mu}' \cdot \mathbf{r}')}{r^5} \right] . \quad (6)$$

The most important contributions to the interaction energy come from distances  $r \approx d$  and relative orientations  $\theta_{ij} \approx 0$ , where  $\theta_{ij}$  denotes the angle between two dipoles contained in a common plane. Thus, magnetic dipoles tend to align in a pole-to-pole configuration while minimizing the interaction energy:

$$U_{\min} = -\frac{\mu_0}{4\pi} \cdot \frac{2\mu\mu'}{d^3} := -\frac{\alpha}{d^3} . \quad (7)$$

where we have introduced the potential parameter  $\alpha$ . An analytical calculation – such as the Rutherford formula for electrostatic interaction – of the collisional cross section  $\sigma_m$  between magnetized dipolar particles is not possible since we are not dealing with a central force problem where the interaction solely depends on the inter-particle distance  $r$ . In general, the

force between two magnetized dust grains will *not* be directed along the line connecting the particles centers. This is equivalent to saying that there is no conservation of angular momentum. However, Eq. 7 can be used to derive an approximate expression for  $\sigma$  since it essentially describes a central potential,  $U = U(r)$ , if we replace the variable  $d$  by  $r$ . Particle motion in this type of potential will be confined to a plane, and orbital angular momentum is conserved. The magnetic moments are assumed to be parallel to a line connecting the particle centers.

Following the treatment of particle motion in a central potential (e.g. LANDAU AND LIFSCHITZ, 1984), scattering of two particles with mass  $m$  can be described in terms of an effective potential

$$U_{\text{eff}}(r) = U(r) + \frac{l^2}{2\bar{m}r^2}, \quad (8)$$

in which we have introduced the reduced particle mass,  $\bar{m} = m^2/2m = m/2$  for identical grains. Equation 8 combines the interaction potential  $U(r)$  given by Eq. 7 and the conservation of orbital angular momentum  $l$ . We are now dealing with an equivalent one-body problem.

For scattering problems,  $l$  is usually given in terms of the impact parameter  $b$ :

$$l = \bar{m} \cdot v_{\infty} \cdot b, \quad (9)$$

where  $v_{\infty}$  denotes the relative velocity prior to interaction, e.g. thermal motion. Combining Eqs. 7 through 9 yields:

$$U_{\text{eff}} = \frac{\bar{m} \cdot b^2 \cdot v_{\infty}^2}{2 \cdot r^2} - \frac{\alpha}{r^3}. \quad (10)$$

We refer to Eq. 7 for a definition of  $\alpha$ . For potentials with  $r^{-2}$ -dependence, the maximum impact parameter can then be derived by simply setting the initial energy  $1/2\bar{m}v_{\infty}^2$  equal to the  $U_{\text{eff}}$  as given by Eq. 10. It should be noted, however, that the effective interaction potential for dipolar interaction (cf. Eq. 10) does not display a *local minimum* as is the case for gravitational or electrostatic interaction, but a *local maximum* given by:

$$U_0 = \frac{1}{2\alpha^2} \cdot \left( \frac{\bar{m} \cdot v_{\infty}^2 \cdot b^2}{3} \right)^3. \quad (11)$$

We therefore obtain  $b_{\max}$  by letting  $E = U_0$ , which implies that an incoming particle first has to cross a potential wall of height  $U_0$  before it can fall into the center of force:

$$\frac{1}{2\alpha^2} \cdot \left( \frac{\overline{m} \cdot v_\infty^2 \cdot b_{\max}^2}{3} \right)^3 \stackrel{!}{=} \frac{\overline{m}v_\infty^2}{2} . \quad (12)$$

Therefore we find for the maximum impact parameter

$$b_{\max} = 3 \cdot \left( \frac{\alpha}{\overline{m}v_\infty^2} \right)^{2/3} . \quad (13)$$

and the magnetic cross section is

$$\sigma_m = 3\pi \cdot \left( \frac{\alpha}{\overline{m}v_\infty^2} \right)^{2/3} . \quad (14)$$

The central-potential approximation necessarily overestimates the magnetic cross section by a factor or order 2, because only maximum interaction is taken into account when deriving Eq. 14.

### 3.2 Accretional remanence

A direct consequence of the increased particle cross section for magnetic grains is the selective coagulation of magnetized dust particles with their kin. Undisturbed magnetic aggregation should lead to the formation of chain-like configurations with very low fractal dimension, since magnetic grains tend to coagulate in a pole-to-pole pattern.  $D_f = 1$  characterizes a perfect chain or rod. With non-magnetic dust grains, aggregation processes in three-dimensional Euclidian space usually result in structures with fractal dimensions around 2 (KEMPF, 1997; WURM AND BLUM, 1998; WURM, 1997; WEIDENSCHILLING *et al.*, 1988). More recently however, BLUM *et al.* (2000) and BLUM AND WURM (2000) reported on the growth of aggregates of SiO<sub>2</sub>-spheres with elongated structures and low fractal dimension ( $D_f = 1.3$  (BLUM *et al.*, 2000)) which can be attributed to rotational effects.

In the case of magnetic grains, chain-like aggregation should coincide with an efficient conservation of the total magnetic moment. For perfectly aligned dipolar particles, the magnetic moment of a chain is given by the sum over

the individual magnetic moments  $\mu_i = \mu$ :

$$\mu_{\text{chain}} = \sum_{i=1}^N \mu_i = N \cdot \mu. \quad (15)$$

For sufficiently high values of the magnetic interaction parameter  $\lambda$  (cf. Eq. 1), i.e.  $\lambda \gg 1$ , there will be no statistical mixing of individual magnetic moments, but – leaving aside thermal agitation and locally disturbed agglomeration due to multi-particle interaction – an increase of the magnetic moment per cluster with the number of constituent particles. This increase  $\mu_{\text{agg}} = \mu_{\text{agg}}(N)$  is called *accretional remanence* (NÜBOLD AND GLASSMEIER, 1999, 2000). Its functional dependence was determined from numerical simulations (NÜBOLD AND GLASSMEIER, 2000) to be

$$\mu_{\text{agg}}(\mu, N) = \mu \cdot N^{0.63}, \quad (16)$$

where  $\mu = \mu_i$  again denotes the magnetic (dipole) moment of a single grain. Large aggregates assembled from thousands of small magnetized grains will therefore still show a large fraction of the total magnetic moment of their constituents.

[Figure 1 about here.]

### 3.3 Aggregation Dynamics

Due to its irreversible character, studies of the the kinetic properties of particle aggregation focus on the dynamic properties of the distribution of clusters. Within this context, the features of aggregation are described in terms of the cluster-size distribution  $n_s(t)$  as a function of time (e.g. MIGUEL AND PASTOR-SATORRAS, 1999, and references therein). As is the case for all distribution functions,  $n_s$  can be used to calculate higher moments, in particular the mean cluster size  $S(t)$  which is defined by:

$$S(t) = \frac{\sum_s s^2 n_s(t)}{\sum_s s n_s(t)}, \quad (17)$$

the variable  $s$  being one particular cluster size from the distribution. The asymptotic behavior of the mean cluster size is a power law

$$S(t) \sim t^z \quad (18)$$

with the so-called *dynamic exponent*,  $z$ , which depends on the aggregation process. For ensembles composed of identical particles, the mean cluster size can be identified with the mean aggregate mass  $m(t)$ .

To our knowledge, the dynamical evolution of magnetic aggregation has never been analyzed before in an astrophysical context, i.e. involving micron-sized particles, low number densities, and a regime of free molecular flow<sup>1</sup>. According to BLUM *et al.* (2000), we expect a behavior (cf. Eq. 18):

$$m(t) \propto t^z \quad (19)$$

for a quasi-monodisperse system. For an ensemble of aggregating particles, the dynamic exponent  $z$  depends on the evolution of the collisional cross section  $\sigma \propto m^\eta$  and of the collision velocity  $v_c \propto m^\nu$ . The exponent  $z$  can be derived using the following equation (BLUM *et al.*, 2000; MEAKIN, 1991):

$$\eta + \nu = \frac{z - 1}{z} . \quad (20)$$

Just like  $m(t)$ ,  $\sigma_c$  and  $v_c$  are assumed to obey power laws. Common dust aggregates have  $D_f = 2$ , therefore  $\sigma_c \propto m$  and  $\eta = 1$ . Thermally induced relative velocities scale with  $m^{-1/2}$ , i.e.  $\nu = -1/2$ . For such systems, we expect to find a dynamic exponent  $z = 2$ .

In magnetically driven coagulation in free molecular flow, particle motion is not diffusive but governed by strong inter-particle forces. For aligned grains with identical dipole moments  $\mu$  we thus have (cf. Eq. 7):

$$v_c \propto \frac{\mu(m)}{\sqrt{m}} . \quad (21)$$

In Eq. 21 we have to insert the functional dependence  $\mu(m)$  of the aggregate dipole moment on the aggregate mass. As shown in the previous section, this dependence has been found in numerical simulations (NÜBOLD AND GLASSMEIER, 2000; NÜBOLD, 1998) to be  $\mu(N) = \mu(m) \propto m^\gamma$  with  $\gamma = 0.63$ . In combination with Eq. 21 we obtain  $v_c \propto m^{0.63} \cdot m^{-1/2} = m^{0.13}$ , i.e.  $\nu \approx 0.13$ .

In contrast to diffusion-limited aggregation, the collisional cross section of magnetic grains is greatly enhanced over the geometric particle size. Again,

---

<sup>1</sup>In the regime of free molecular flow, the mean free path of the molecules of the embedding medium (gas) is greater than the size of the dust particles under consideration.

for perfectly aligned dipoles we have:

$$\begin{aligned}\sigma_c &\propto (m^\gamma)^{4/3}, \\ &= (m^{0.63})^{4/3},\end{aligned}\tag{22}$$

thence  $\eta \approx 0.84$ .

Since the foregoing derivations of  $\nu$  and  $\eta$  imply maximum magnetic interaction, these values have to be considered as strict upper limits. To treat this problem in a more quantitative manner, we shall include the increasing dipole relaxation time  $\tau(m)$ , i.e. the characteristic mass-dependent time scale for dipole alignment.

The relaxation time  $\tau$  associated with a rotation of dipoles, e.g. through an angle  $\varphi = \pi/2$ , can be estimated from:

$$\tau \propto \sqrt{\frac{\varphi}{\dot{\omega}}} \sim \sqrt{\frac{I}{M}} \sim \sqrt{\frac{m^2}{\mu(m)^2}},\tag{23}$$

where  $\dot{\omega}$ ,  $I$ , and  $M$  denote the magnetic angular acceleration, the moment of inertia of the aggregate, and the magnetic inter-particle torque, respectively. Thus we obtain  $\tau \propto \sqrt{m^{2 \cdot (1-0.63)}} = m^{0.37}$ . If we include this aspect in our calculation of the exponents  $\nu$  and  $\eta$ , we find the alignment-corrected values  $\nu^*$  and  $\eta^*$  by replacing  $\mu^2$  in Eq. 7 with  $\mu^{2-0.37} = \mu^{1.63}$  to account for imperfect alignment. The results are:

$$\nu^* \approx 0.01,\tag{24}$$

$$\eta^* \approx 0.68.\tag{25}$$

Insertion of  $\eta^*$  and  $\nu^*$  into Eq. 20 yields  $z \approx 3.2$ . This value for the dynamic exponent should characterize the kinetics of magnetic dust aggregation. It is the direct consequence of the combined effects of enhanced collisional cross sections and accretional remanence.

## 4 Simulations using *SAND*: Two test cases

A thorough analysis of the intricate microphysics of magnetic aggregation requires numerical tools which are able to treat both long-range magneto-static and short-range surface forces for large particle systems. To this end,

we devised a new coagulation code called *SAND*. Please refer to Sect. A for a detailed description of the program which was also used for additional numerical simulation of magnetic coagulation. The results of this work will be the subject of a subsequent paper. In this section, we present two test cases which are meant to illustrate the abilities of *SAND*.

## 4.1 Cross sections

To test the validity of our theoretical treatment of magnetic aggregation, we performed detailed one-on-one scattering simulations, in which one dipole is magnetically deflected or attracted in the field of an identical, initially motionless, counterpart.

For a detailed study of magnetic cross sections, we systematically varied the impact parameter around the value  $b_{\max}$  as given by Eq. 13. We are thus able to determine the maximum value for collisions at different initial relative velocities  $v_{\infty}$ , which were taken from a Maxwellian distribution at 100 K ( $0.3 \cdot v_{th} \leq v_{\infty} \leq 3 \cdot v_{th}$ ).

[Figure 2 about here.]

[Figure 3 about here.]

For all configurations  $[v_{\infty}, b]$  we randomly chose the initial orientations  $(\theta_i, \phi_i)$  of the two scattering dipoles, which were placed at a relative distance as given by Eq. 2. Figure 2 shows three example trajectories. Only the first scattering calculation with an impact parameter  $b = 0.95 \cdot b_{\max}$  leads to a “hard” collision of the grains. The second calculation with an impact parameter  $b = b_{\max}$  does not lead to a “hard” collision. Instead we see that the two grains almost entirely exchange their energy and momentum. The impacting grain is moving only very slowly after the collision, while the grain initially at rest leaves the scene at a speed comparable to the impactor’s initial velocity. In Fig. 2, different velocities are represented by different spacing of dots along the trajectory. For the third calculation with  $b = 1.05 \cdot b_{\max}$ , the grains do not hit each other and there is only partial transfer of energy. These three calculations therefore show good qualitative agreement between the predicted cross section (c.f. Eq. 14) and the numerical result.

Figures 3(a,b) analyze the results of a large number of simulations in a quantitative way, using color coding to account for orientation dependent



collision probabilities. While the detailed values are generally smaller than those obtained previously (NÜBOLD AND GLASSMEIER, 1999, 2000), the qualitative agreement is good. At  $v_{th} = \sqrt{k_B T/m}$  we find:

$$\frac{\sigma_m}{\sigma}(v_\infty = v_{th}) \approx 130. \quad (26)$$

The discrepancy between the two results presented in Eq. 5 and Eq. 26 can be interpreted as a direct measure of the effect of the degree of magnetic alignment, although it should be noted that a small part of the discrepancy is due to the change in temperature (80 K vs. 100 K). According to Eq. 14,  $\sigma_m$  scales with  $T^{-2/3}$ . The temperature-corrected value for  $\sigma_m$  in Eq. 26 should therefore be approximately  $130 \cdot 0.8^{-2/3} \approx 151$ . The numerical values equally validate Eq. 14. As had to be expected, the theoretically derived value for  $\sigma_m$  – the dashed line in Fig. 3 – is too big, since only maximum interaction enters the central-force approximation. Orientation averaged collision probabilities reach 100% at smaller impact parameters that can be estimated from the outer radius of the white annuli,  $R_w$ . This can be accounted for by introducing an empirical correction factor  $c = (R_w/R_{dash})^2$  in Eq. 14:

$$\sigma_m = c \cdot 3\pi \left( \frac{\alpha}{m v_\infty^2} \right)^{2/3}. \quad (27)$$

By inspection of Fig. 3 we estimate  $c$  to lie between 0.8 and 0.9, i.e. the approximation error in Eq. 14 is of the order of 10-20%. We do not see a strong velocity dependence of this correction factor.

[Figure 4 about here.]

## 4.2 Restructuring and contact forces

The long-range interactions between magnetized dust grains give rise to an increase in inter-particle collision velocities which have to be accounted for in realistic coagulation models. Figure 4 illustrates the importance of including configurational flexibility and means for aggregate restructuring in coagulation models. Model calculations of dust coagulation usually dwell on very few assumptions, sometimes neglecting the aggregate structure altogether. The simplest approach treats grain growth in analogy to the coagulation of liquid drops, where the combination of two drops leads to the formation of

one – bigger – drop. Next in complexity are “hit-and-stick” models (e.g. WEIDENSCHILLING AND RUZMAIKINA, 1994; OSSENKOPF, 1993; MEAKIN AND DONN, 1988) where grains are assumed to stick where they hit, whence the name, and do not influence the aggregate structure. While the particle trajectories may be either ballistic (e.g. OSSENKOPF, 1993)) or stochastic, i.e. pseudo-ballistic with random changes of direction on a diffusion-controlled time scale (KEMPF, 1997), there is no aggregate restructuring during collisions. Some models include sticking probabilities (OSSENKOPF, 1993) whereas others prescribe fixed values for the fractal dimension at different stages of the simulation (WEIDENSCHILLING *et al.*, 1988). A realistic treatment of aggregates as solid bodies has been given by RICHARDSON (1995).

The detailed analysis of inter-particle contact forces by DOMINIK AND TIELENS (1997) allows a more consistent approach. Clusters of particles are no longer treated as separate objects that must be parameterized with respect to their physical properties, rather they preserve their identity and are considered under the influence of all forces transmitted through each grain’s contacts with adjacent particles. Especially when strong inter-particle forces are involved, grain-grain collisions can be violent and produce intricate results. This is shown in Fig. 4 where the linear aggregate is restructured to a T-shape after the fast impact of another grain.

## 5 Conclusions

The material presented in this paper lays the foundation for a detailed analysis of the effects of magnetic aggregation for the accumulation of solid matter in the early solar system. Generalizing previous work by NÜBOLD AND GLASSMEIER (1999, 2000), we have derived an analytical expression for the collisional (capture) cross section of magnetic dust grains. As pairs of dipolar magnetic particles tend to line up in pole-to-pole configuration, aggregates of such particles “preserve” the magnetic moment of their constituents, thus displaying “accretional remanence”. The combination of enhanced cross section and accretional remanence is responsible for accelerated growth dynamics. This fact is quantitatively described by a dynamic exponent,  $z$ , such that the temporal dependence of the mean aggregate mass,  $m$ , takes on the form of a power law, i.e.,  $m \propto t^z$ . We have shown that the dynamic exponent takes on a value  $z \approx 3.2$  for magnetic aggregation, whereas  $z = 2$  for aggregation

processes with non-magnetic particles.

Part of our theoretical approach has been validated numerically as a means for introducing a new coagulation code which we devised for the detailed analysis of magnetic coagulation. Its architecture allows the study of systems of particles interacting via long-range magnetostatic coupling as well as through short-range elastic forces. Aggregate restructuring is included. We provide evidence that such an approach – although computationally rather costly - is required for physically realistic modelling. A forthcoming paper will present extensive numerical studies of magnetic aggregation.

**Acknowledgements:** We would like to thank Tijmen van de Kamp for the development of Grainview, an interactive tool to visualize aggregate simulations; Vincent Icke and Kees Dullemond for discussions about how to implement grain rotation, Josef Schüle for help with optimizing the code. CD acknowledges financial support from Pioneer grant 600-78-333. HN acknowledges financial support from the Studienstiftung des Deutschen Volkes and from DFG grant GL 142/13-1.

## A The *SAND* code

*SAND* (Soft Aggregate Numerical Dynamics) is a code to compute the aggregation of dust particles in a detailed way, treating the microphysics of the contacts between dust particles, long range forces like magnetic dipole and electrostatic interactions, and external forces like external magnetic or gravitational fields. This is a new combination which in this way has not been used before. The precursor of *SAND* was the 2D code used by DOMINIK AND TIELENS (1997) to study the behavior of dust aggregates in collisions, but without long-range forces.

*SAND* treats aggregates of dust grains as N-particle systems. Each individual grain is free to move under the forces acting on it. Such forces can be due to external fields, to long-range grain-grain interactions, and to mechanical force transmission through physical contacts between grains.

*SAND* currently treats only spherical particles, but an extension to spheroids or ellipsoids would be possible.

*SAND* was originally written to treat contact forces only, and therefore was best suited to study the collision of aggregates. Full aggregation calculations were not possible because the detailed numerical treatment of the contacts imposes very short time steps, of the order of  $10^{-11}$  seconds in or-

der to resolve the vibrational motion of grains in contact. Long-range forces considerably shorten the growth-time for an aggregating particle system. It therefore becomes feasible to conduct coagulation calculations with the code. On the other hand, implementing long-range forces also brings up the following challenges.

- For long-range forces, every particle in an  $N$ -particle numerical simulation interacts with *all other particles*, thus leading to an  $N^2$  scaling for the computation time. If only contact forces are involved, the code is linear in  $N$ .
- Some kind of boundary condition has to be introduced in order to model the interaction of “edge particles”, i.e. particles close to the edge of the spatially limited simulation volume. For forces of virtually unlimited range, this can be a serious complication.
- As interaction forces are strongly dependent on the inter-particle distance, interaction between grains that are far apart will be treated in too much detail – numerically speaking – if only one global simulation time step is used. This problem is of particular importance in the case of *SAND*, since strong contact forces require very small time steps in the numerical treatment of the differential equations involved.

*SAND* tackles these problems by means of a list-based interaction calculation for long-range forces and a multiple time step algorithm, that separates short-range contact forces from long-range dipolar interaction.

In the following we describe briefly the equations solved by *SAND*. Two test calculations are discussed in Sect. 4. More detailed simulations of magnetic accretion will be the subject of a forthcoming paper.

## A.1 Grain properties

Each individual grain  $i$  is described by material properties (specific density  $\rho_i$ , surface energy  $\gamma_i$ ), radius  $a_i$ , mass  $m_i$ , moment of inertia  $I_i$ , magnetic moment vector  $\boldsymbol{\mu}_i$ . The state of each particle is given by a location  $\boldsymbol{r}_i$ , a velocity  $\boldsymbol{v}_i$ , rotational state  $\boldsymbol{\varrho}_i$ , and by a rotation velocity  $\boldsymbol{\omega}_i$ .

## A.2 Linear Motion

The differential equations describing the linear motion of each grain are simply

$$\dot{\mathbf{r}}_i = \mathbf{v}_i \quad (28)$$

$$\dot{\mathbf{v}}_i = \mathbf{F}_{i,\text{contact}} + \mathbf{F}_{i,\text{magnetic}} . \quad (29)$$

$\mathbf{F}_{i,\text{contact}}$  is the sum of all linear elastic forces transmitted through contacts involving grain  $i$ .  $\mathbf{F}_{i,\text{magnetic}}$  is the sum of all magnetic interactions of grain  $i$  with other grains and an external magnetic field. In a similar way, gravitation and electrostatic forces could be added, but this is not relevant for our current study.

## A.3 Rotation

The rotational state  $\boldsymbol{\varrho}_i$  is a four-vector which contains the rotation parameters  $\varrho_{i,1}$ ,  $\varrho_{i,2}$ ,  $\varrho_{i,3}$ , and  $\varrho_{i,4}$  which can be used to describe the rotation of a solid body by differential equations, avoiding the singularities characteristic for Eulerian angles and similar 3-parameter representations. We follow the formalism by WHITTAKER (1904).

Grains initially enter the calculations with parameters  $\boldsymbol{\varrho}_i(t_0) = (0, 0, 0, 1)$ . At a later state,  $\boldsymbol{\varrho}_i(t) = (\varrho_{i,1}(t), \varrho_{i,2}(t), \varrho_{i,3}(t), \varrho_{i,4}(t))$ . The new orientation can be computed from the old orientation by a single rotation using the rotation matrix

$$\mathcal{R}_i(t) = \begin{pmatrix} \varrho_{i,1}\varrho_{i,1} - \varrho_{i,2}\varrho_{i,2} - \varrho_{i,3}\varrho_{i,3} + \varrho_{i,4}\varrho_{i,4} & 2(\varrho_{i,1}\varrho_{i,2} - \varrho_{i,3}\varrho_{i,4}) & 2(\varrho_{i,1}\varrho_{i,3} + \varrho_{i,2}\varrho_{i,4}) \\ 2(\varrho_{i,1}\varrho_{i,2} + \varrho_{i,3}\varrho_{i,4}) & -\varrho_{i,1}\varrho_{i,1} + \varrho_{i,2}\varrho_{i,2} - \varrho_{i,3}\varrho_{i,3} + \varrho_{i,4}\varrho_{i,4} & 2(\varrho_{i,2}\varrho_{i,3} - \varrho_{i,1}\varrho_{i,4}) \\ 2(\varrho_{i,1}\varrho_{i,3} - \varrho_{i,2}\varrho_{i,4}) & 2(\varrho_{i,2}\varrho_{i,3} + \varrho_{i,1}\varrho_{i,4}) & -\varrho_{i,1}\varrho_{i,1} - \varrho_{i,2}\varrho_{i,2} + \varrho_{i,3}\varrho_{i,3} + \varrho_{i,4}\varrho_{i,4} \end{pmatrix}, \quad (30)$$

where we have omitted the time arguments for brevity. This matrix can be used to rotate any vector properties of the particle, such as the magnetic moment into the current state.

The differential equations for the rotation parameters are given by

$$\begin{aligned}
\dot{\varrho}_{i,1} &= (\varrho_{i,4}\omega_{i,1} + \varrho_{i,3}\omega_{i,2} - \varrho_{i,2}\omega_{i,3})/2 \\
\dot{\varrho}_{i,2} &= (\varrho_{i,4}\omega_{i,2} - \varrho_{i,3}\omega_{i,1} + \varrho_{i,1}\omega_{i,3})/2 \\
\dot{\varrho}_{i,3} &= (\varrho_{i,2}\omega_{i,1} - \varrho_{i,1}\omega_{i,2} + \varrho_{i,4}\omega_{i,3})/2 \\
\dot{\varrho}_{i,4} &= -(\varrho_{i,3}\omega_{i,3} + \varrho_{i,2}\omega_{i,2} + \varrho_{i,1}\omega_{i,1})/2 .
\end{aligned} \tag{31}$$

The rotation parameters also must fulfill a normalization condition, i.e.

$$\varrho_{i,1}^2 + \varrho_{i,2}^2 + \varrho_{i,3}^2 + \varrho_{i,4}^2 = 1 . \tag{32}$$

Solving the differential Eq. 31 introduces numerical errors into the rotation parameters. After each successful timestep, we therefore re-normalize the rotation parameters in accordance with Eq. 32.

The differential equation for the change of the angular velocity  $\boldsymbol{\omega}$  is simply

$$\dot{\boldsymbol{\omega}}_i = \mathbf{M}_{i,\text{contact}} + \mathbf{M}_{i,\text{magnetic}} , \tag{33}$$

where  $\mathbf{M}_{i,\text{contact}}$  is the sum of all elastic torques transmitted through contacts involving grain  $i$ .  $\mathbf{M}_{i,\text{magnetic}}$  is the torque due to all magnetic interactions of the grain  $i$  with other grains and with an external magnetic field.

## A.4 Magnetic forces

The basic equation for the magnetostatic interaction between two dipolar particles has been given in Sect. 3.1 (cf. Eq. 6). For notational simplicity, we let the constant factor  $(\mu_0/4\pi) = 10^{-7}$  be equal to 1 for the remainder of this section. The derivation of the force acting between two magnetic dipoles  $i, j$  is straightforward. In three-dimensional Cartesian coordinates, we have:

$$\mathbf{F}_{ij} = (\boldsymbol{\mu}_j \boldsymbol{\nabla}) \mathbf{B}_{ij} . \tag{34}$$

In Eq. 34, the double subscript  $ij$  describes the influence of particle  $i$  on particle  $j$ , i.e. at the location of particle  $j$ . Individual particles are referred to by single subscripts, e.g.  $i$ .

Carrying out the multiple differentiations in Eq. 34 and introducing the relative distance vector,  $\mathbf{r}_{ij}$ , of length  $r$  we have:

$$\mathbf{F}_{ij} = \frac{3}{r^5} \left[ \mathcal{M}_1 - \frac{5(\boldsymbol{\mu}_i \cdot \mathbf{r}_{ij})}{r^2} \cdot \mathcal{M}_2 \right] \cdot \boldsymbol{\mu}_j , \tag{35}$$

$$\text{with } \mathcal{M}_1 = \boldsymbol{\mu}_i \cdot \mathbf{r}_{ij}^T + \mathbf{r}_{ij} \cdot \boldsymbol{\mu}_i^T + (\boldsymbol{\mu}_i \cdot \mathbf{r}_{ij}) \cdot \mathcal{I} , \tag{36}$$

$$\text{and } \mathcal{M}_2 = \mathbf{r}_{ij} \cdot \mathbf{r}_{ij}^T . \tag{37}$$

In Eqs. 36 and 37, the superscript  $T$  denotes a row vector. The matrix  $\mathcal{I}$  in Eq. 36 is the identity matrix. All matrices contained in Eqs. 35-37 are symmetric, i.e., for actual computation only six out of nine elements have to be calculated. Trivially,  $\mathbf{F}_{ji} = -\mathbf{F}_{ij}$ .

Apart from translational forces, dipoles will also exert torques  $\mathbf{M}_{\text{int}}$  on their counterparts. Each contribution  $\mathbf{M}_{ij,\text{int}}$ , i.e. the torque acting on dipole  $j$  in the magnetic (dipole) field due to particle  $i$  at the location of  $j$ , is given by

$$\mathbf{M}_{ij,\text{int}} = \boldsymbol{\mu}_j \times \mathbf{B}_{ij} \quad (38)$$

$$= \boldsymbol{\mu}_j \times \left[ 3 \frac{\mathbf{r}_{ij} \cdot (\boldsymbol{\mu}_i \cdot \mathbf{r}_{ij})}{r^5} - \frac{\boldsymbol{\mu}_i}{r^3} \right]. \quad (39)$$

In addition to mutual interaction (cf. Eq. 39), magnetic grains can interact with an external magnetic field  $\mathbf{B}_{\text{ext}}$ . As a result of an undamped interaction the perpendicular part of the magnetic dipole moment vector of each grain,  $\boldsymbol{\mu}_j^* = \boldsymbol{\mu}_{j,\perp} \mathbf{B}$ , will oscillate around the direction of the external field. The magnetic torque  $\mathbf{M}_{j,\text{ext}}$  causing this oscillation is given by

$$\mathbf{M}_{j,\text{ext}} = \boldsymbol{\mu}_j \times \mathbf{B}_{\text{ext}}, \quad (40)$$

$$|\mathbf{M}_{j,\text{ext}}| = \boldsymbol{\mu}_j^* \cdot \mathbf{B}_{\text{ext}}. \quad (41)$$

In the scope of *SAND*, the external magnetic field will be constant in time and – without loss of generality – directed along the  $z$ -direction.

## A.5 Contact forces

When two grains collide, they can form a contact. Forces are transmitted through such contacts, and the magnitude of these forces largely determines the structure and mechanical properties of an aggregate. A contact between two grains has an equilibrium state in which the attractive forces are balanced by elastic forces due to compression of the material near the contact (DOMINIK AND TIELENS, 1995, 1996, 1997). Dynamic forces on the grains lead to additional stresses in the contact area which are responsible for contact forces acting on the two grains. As long as the forces do not exceed the elastic regime, the contact forces can be calculated as a function of the displacement of the grains from the equilibrium contact position. Therefore, the problem of computing contact forces is reduced to computing these displacements. If the elastic limits of the contact are exceeded, the contact

breaks or moves, and energy is dissipated in this process. In the following we describe the procedure which is used in *SAND* to keep track of contact locations and displacements.

When a new contact between grains  $i$  and  $j$  is formed, we define the following vectors describing the position of the contact on each grain. Let  $\mathbf{c}$  denote the position where the grain surfaces touch. In the program, this defines a new contact structure which is kept in a list. We define a vector  $\mathbf{P}_1 = \mathbf{c} - \mathbf{r}_i$  which points from the center of grain  $i$  to the contact point and a vector  $\mathbf{P}_2 = \mathbf{c} - \mathbf{r}_j$  which points from the center of grain  $j$  to the contact point. We also define a unit vector  $\mathbf{Q}$  which is perpendicular to the line connecting the two grain centers:  $|\mathbf{Q}| = 1$  and  $\mathbf{Q} \cdot (\mathbf{r}_i - \mathbf{r}_j) = 0$ .

[Figure 5 about here.]

At a later stage during the calculation, the two grains  $i$  and  $j$  have moved so that their positions and/or rotational states are different.

If a contact were treated as being entirely rigid, the grains could only move such that the contact remains in its original position on the connecting line. This corresponds to a treatment of aggregates as rigid solid bodies (RICHARDSON, 1995). However, both grains are still treated as individual particles and they can move in a different way. If the contact is not lost, the material near the contact is strained in order to accommodate the small differences from rigid body motion. We can now use the vectors  $\mathbf{P}_1$ ,  $\mathbf{P}_2$ , and  $\mathbf{Q}$  to compute how much the material has been strained. Figure 5 shows the definition of these vectors. The displacements can then be calculated in the following way. First we rotate the vectors  $\mathbf{P}_1$ ,  $\mathbf{P}_2$ , and  $\mathbf{Q}$  into the new orientations of the grains, using the current rotation matrices

$$\mathbf{p}_1 = \mathcal{R}_i \mathbf{P}_1 \quad , \quad \mathbf{p}_2 = \mathcal{R}_j \mathbf{P}_2 \quad , \quad \mathbf{q}_1 = \mathcal{R}_i \mathbf{Q} \quad , \quad \mathbf{q}_2 = \mathcal{R}_j \mathbf{Q} . \quad (42)$$

The total linear displacement between the contact pointers is the vector

$$\boldsymbol{\delta} = \mathbf{r}_j + \mathbf{p}_2 - \mathbf{r}_i - \mathbf{p}_1 . \quad (43)$$

We define a unit vector pointing from the center of grain  $j$  to the center of grain  $i$

$$\mathbf{e}_\perp = \frac{\mathbf{r}_1 - \mathbf{r}_2}{|\mathbf{r}_1 - \mathbf{r}_2|} \quad (44)$$



and compute the linear displacement in the direction of the inter-grain axis  $\boldsymbol{\delta}_\perp$  (pulling degree of freedom) and the displacement in the contact plane  $\boldsymbol{\delta}_\parallel$  (sliding degree of freedom) with

$$\boldsymbol{\delta}_\perp = (\boldsymbol{\delta} \cdot \mathbf{e}_\perp) \mathbf{e}_\perp \quad (45)$$

$$\boldsymbol{\delta}_\parallel = \boldsymbol{\delta} - \boldsymbol{\delta}_\perp . \quad (46)$$

Due to rolling of the surfaces over each other, the center of the contact area is displaced from the inter-grain axis by

$$\boldsymbol{\xi} = \frac{(\mathbf{p}_1 - \mathbf{p}_2) \times (\mathbf{p}_1 \times \mathbf{p}_2)}{(\mathbf{p}_1 - \mathbf{p}_2)^2} . \quad (47)$$

Finally we can compute the relative angular displacement around the inter-grain axis  $\alpha_\parallel$  (twisting degree of freedom) and around an axis in the contact plane but perpendicular to the  $\boldsymbol{\xi}$  vector:  $\alpha_\perp$  (rolling degree of freedom).

$$\alpha_\parallel = \arcsin(\mathbf{q}_1 \times \mathbf{q}_2 \cdot \mathbf{e}_\perp) \quad (48)$$

$$\alpha_\perp = \arccos(\mathbf{p}_1 \cdot (-\mathbf{p}_2)) . \quad (49)$$

From these displacements, the forces and torques acting on the grains can be directly computed using the formalism described by DOMINIK AND TIELENS (1997), with the following modifications:

- HEIM *et al.* (1999) and BLUM AND WURM (2000) have shown that the critical rolling displacement  $\xi_{\text{crit}}$  is of the order of 10-20Å instead of 1Å as used by DOMINIK AND TIELENS (1997). For the calculations in this paper, we have used  $\xi_{\text{crit}} = 10\text{Å}$ . Rolling is the dominant restructuring process in the simulations in this paper, and a proper treatment is important here. The measurements by Blum and Wurm have been restricted to Quartz particles, so the application to metallic or ceramic particles introduces some uncertainty.
- POPPE *et al.* (2000) have shown experimentally that the critical velocity for sticking can be considerably higher than the value predicted by CHOKSHI *et al.* (1993). This has to be interpreted as an additional channel of energy dissipation which is not yet well understood. Since there is no good theoretical description available, we have still used the lower energies and velocities for sticking. In the current study this effect is probably not of critical importance since the attraction between grains is dominated by magnetic forces and generally leads to immediate sticking.

## A.6 Restructuring: making, breaking, moving contacts

The algorithm described in the previous section is the one used while contacts are in the elastic regime. In this regime, the aggregate keeps its basic shape except for minor bending and stretching. When the dynamic forces acting on grains in contact become too big, the contact will start to move over the two grains by rolling or sliding, or it will break. Within each time step, *SAND* assumes all contacts to be stable and elastic, in order to make it possible for the integrator to work on a set of continuous functions. This assumption limits the time step possible for *SAND* to the period of the fastest contact vibration. After each timestep, *SAND* checks if any of the contacts are strained too much. If this is the case and the grains are too far apart to stay in contact, the contact is broken and removed from the internal list. If the grains are still close enough to touch, the contact is moved to a new equilibrium location, releasing the stresses that prompted the motion. Then new values for the contact vectors  $\mathbf{P}_1$ ,  $\mathbf{P}_2$ , and  $\mathbf{Q}$  are computed and the time integration continues. Also after each time step, the integration volume is checked for grains which have approached each other so that a new contact has to be established.

## A.7 List algorithm

An  $N$ -particle code with long-range forces can only be numerically efficient, if we can cut down the  $\mathcal{O}(N^2)$ -dependence to a more acceptable  $\mathcal{O}(N)$ -dependence. To within a numerical factor, this obviously represents the lower bound for the amount of work required to process all  $N$  particles.

In Eq. 2, we defined a thermally induced interaction limit for dipolar magnetic coupling. We can thus effectively reduce the long-range interaction of a given dipole  $j$  to that with a restricted set of *neighbor* particles. The computational problem is now reduced to implementing an efficient algorithm for list construction and maintenance. We have used a cell subdivision (RAPAPORT, 1995) adapted for the use with magnetically interacting grains.

We use Eq. 2 as a definition for the *cut-off distance*,  $r_c$ , for our long-range forces. The simulation space is subdivided into cells whose (identical) edges all exceed  $r_c$  in length. Interaction is only possible if two grains are either in the same cell or in immediately adjacent (nearest neighbors) cells. In three dimensions, each cell has 26 neighboring cells. Due to reasons of symmetry only half of these need be considered. Note that this method only works

properly if the size simulation volume exceeds  $4r_c$ . Since we do not know in advance how many particles will occupy a given cell at any instant, linked lists (RAPAPORT, 1995) are used to associate particles with the cell they reside in.

The cell method can be considerably refined by a neighbor-list method. For cells with an edge length  $r_c$ , on the average only a small fraction of the examined particles lie within interaction range. In order to make use of this reduced neighborhood size, we have to construct a list of interacting pairs from the set of particles found by the cell method. To this end, we replace the cut-off distance  $r_c$  by  $r_c + \Delta r$  with  $\Delta r > 0$  in order to allow the neighbor-list to be useful during several numerical time steps,  $\Delta t_i$ . The concise value of  $\Delta r$  is related to the rate at which the list has to be updated in an inverse fashion. The list is updated whenever the cumulative maximum velocity  $\mathbf{v}_{\max}$  exceeds a certain limit:

$$\sum_{\Delta t_i} |\mathbf{v}_{i,\max}| > \frac{\Delta r}{\Delta t_i}. \quad (50)$$

This is a rather conservative criterion since it sums contributions from different particles. In practice,  $\Delta r$ -values between  $0.3r_c$  and  $0.4r_c$  have proved useful. For the evaluation according to Eq. 50 only unbound grains are considered. Bound particles are subject to strong elastic forces (DOMINIK AND TIELENS, 1997) that cause rapid oscillation.

In order to include long-range forces on particles close to the edge of the simulation volume, “wraparound” boundary conditions have been implemented into *SAND*.

For an ensemble of 100 magnetic particles, the combined cell-based neighbor-list method leads to a decrease in computation time by a factor of 30 to 40. Since our approach is validated not only on a numerical basis but also with respect to physical considerations we have implemented an efficient way of dealing with magnetic forces in an  $N$ -particle simulation.

## A.8 Multiple time scales

Based on the considerations in the last section, dipolar magnetic interaction of thermalized grains, i.e. grains that are subject to random thermal motion and rotation, can be viewed as moderately long-ranged with cut-off distance  $r_c$ . On these grounds the *complete set* of  $N(N - 1)/2$  pair interactions can

be divided into a so-called *cardinal set* which contains all pairs  $(i, j)$  for which  $d_{ij} \leq r_c$ , and the so-called *inessential set* for which interactions are neglected (STREETT *et al.*, 1977). The population of both the cardinal and the inessential sets change with time.

The multiple time step (MTS) approach focuses on the point that the cardinal set can be subdivided into classes of *primary* and *secondary* neighbors based on a distance criterion for potentials with strong  $r$ -dependence. It is the rapidly changing force due to the primary neighbors that sets an upper limit for the time-step  $\Delta t$  in the simulation. In the MTS method, only the contributions of these primary neighbors are updated at every step. Longer time-steps are used to calculate the evolution of the secondary force, i.e. the contribution due to the secondary neighbor particles. To achieve this, the secondary force at time  $t = t_0 + k\Delta t$  is calculated from a Taylor series expansion based on information at a given time  $t_0$ :

$$\mathbf{F}_s(t_0 + k\Delta t) = \mathbf{F}_s(t_0) + \sum_m \mathbf{F}_s^{(m)}(t_0) \frac{(k\Delta t)^{(m)}}{m!}, \quad (51)$$

where the superscript  $(m)$  denotes the differentiation with respect to time. A similar equation could be written down for the torque,  $\mathbf{M}$ . Equation 51 is referred to as the  $m$ th-order Taylor series. The maximum value  $k_{\max}$  for the parameter  $k$  has to be chosen in such a way that the gain in computational efficiency balances the loss in numerical accuracy. During the simulation,  $k$  runs from 1 to  $k_{\max}$ . At that point a new Taylor series is calculated according to Eq. 51 and that step becomes the new  $t_0$ .

While using additional memory for the storage of Taylor expansions, this method can achieve an additional increase in computational speed for all but the smallest systems up to a factor of five (STREETT *et al.*, 1977). The authors also report on the numerical error as a function of the expansion order  $m$  and the parameter  $k_{\max}$ .

In our coagulation model, an MTS approach is already inherent in the numerical setup. In the scope of *SAND*, we identify the elasto-mechanical contact forces with the primary force and the magnetic forces with the secondary force. Since we use an adaptive step size algorithm to integrate the equations of motion, the step length  $\Delta t$  is automatically adapted to the “physical” situation based on a prescribed absolute error criterion. As soon as the first inter-particle contact is formed, the average step size drops by a factor of  $10^2$  due to the strong elastic forces acting on only a few particles.

At this point we call upon the MTS method, which has been implemented as an optional feature into *SAND*.

Although straightforward mathematically, the calculation of the Taylor expansion for magnetic dipole-dipole interaction is a rather cumbersome task for  $\mathbf{F}_{ij} = \mathbf{F}_{ij}(\boldsymbol{\mu}_i, \boldsymbol{\mu}_j, \mathbf{r}_{ij})$ . As before, the vector  $\mathbf{r}_{ij}$  denotes the relative position of the two dipoles involved. In what follows we shall drop the superscript ( $ij$ ) for simplicity's sake. Unless otherwise noted all vector quantities are assumed to originate from particle  $i$  and to be directed toward or acting upon particle  $j$ . The basic formula involved is:

$$\dot{\mathbf{F}} = \underbrace{\frac{\partial \mathbf{F}}{\partial \mathbf{r}}}_{:=\mathcal{J}_r} \cdot \frac{\partial \mathbf{r}}{\partial t} + \sum_{k=i,j} \underbrace{\frac{\partial \mathbf{F}}{\partial \boldsymbol{\mu}_k}}_{:=\mathcal{J}_{k,\mu}} \cdot \frac{\partial \boldsymbol{\mu}_k}{\partial t}, \quad (52)$$

which is the total time derivative of the dipolar force. Since *SAND* solves the full set of equations for particle motion including rotation, the vectors  $\dot{\boldsymbol{\mu}}_k$  are simply given by  $|\boldsymbol{\mu}_k| \cdot \boldsymbol{\omega}_k$  if  $\boldsymbol{\omega}_k$  denotes the angular velocity of the grain.  $\mathbf{v}$  is the translational velocity of the particle. The matrices  $\mathcal{J}_r$  and  $\mathcal{J}_{k,\mu}$  are the *Jacobian matrices*.

The Taylor expansion for the magnetic torque has to incorporate both internal and external contributions. As before, we drop the subscript  $ij$ . The expression for the first time derivative of the torque  $\dot{\mathbf{M}}_j$  due to internal interaction then reads:

$$\dot{\mathbf{M}}_{j,\text{int}} = \frac{\partial \boldsymbol{\mu}_i}{\partial t} \times \mathbf{B} + \boldsymbol{\mu}_i \times \frac{\partial \mathbf{B}}{\partial t}. \quad (53)$$

The expression for the dipolar magnetic field  $\mathbf{B}$  has been stated before (cf. Eq. 39). In analogy with Eq. 52, the time variation of the magnetic field,  $\partial \mathbf{B} / \partial t$ , can be determined from

$$\dot{\mathbf{B}} = \mathcal{J}_r \dot{\mathbf{r}} + \mathcal{J}_{i,\mu} \dot{\boldsymbol{\mu}}_i. \quad (54)$$

The external contribution for each magnetic grain is simply given by:

$$\dot{\mathbf{M}}_{j,\text{ext}} = |\boldsymbol{\mu}_j| \cdot \boldsymbol{\omega}_j \times \mathbf{B}_{\text{ext}}. \quad (55)$$

We therefore use the following expression for the total time derivative of the magnetic torque on a given particle  $j$  which can be derived by combining Eqs. 53-55:

$$\dot{\mathbf{M}}_j = \dot{\boldsymbol{\mu}}_j \times \mathbf{B} + \boldsymbol{\mu}_j \times (\mathcal{J}_r \dot{\mathbf{r}} + \mathcal{J}_{i,\mu} \dot{\boldsymbol{\mu}}_i) + |\boldsymbol{\mu}_j| \cdot \boldsymbol{\omega}_j \times \mathbf{B}_{\text{ext}}. \quad (56)$$

In our numerical work, Taylor series expansions have been constrained to first order due to the rather complicated structure of the derivatives. These are recalculated at  $t_0$  according to Eqs. 52 and 56. During the following  $k_{\max}$  time steps, which are governed by the high numerical demands of strong contact forces, all magnetic forces are calculated using Eq. 51 and its counterpart for the torques. In practice, the choice  $k_{\max} = 70$  has yielded satisfactory results both in terms of computing time and physical accuracy.

## References

- BALL, R. C. AND WITTEN, T. A., 1984. Causality Bond on the Density of Aggregates. *Phys. Rev. A* **29**, 2966–2967.
- BECKWITH, S. V. W., HENNING, T., AND NAKAGAWA, Y., 2000. Dust properties and assembly of large particles in protoplanetary disks. In *Protoplanets and Planets IV* (Edited by V. Mannings, A. P. Boss, and S. S. Russell), pp. 533+, Tucson. University of Arizona Press.
- BLUM, J. . AND WURM, G., 2000. Experiments on sticking, restructuring, and fragmentation of preplanetary dust aggregates. *Icarus* **143**, 138–146.
- BLUM, J., WURM, G., KEMPF, S., *et al.*, 2000. Growth and form of planetary seedlings: Results from a microgravity aggregation experiment. *Physical Review Letters* **85**, 2426–2429.
- BOSS, A. P., 1996. A concise guide to chondrule formation models. In *Chondrules and the Protoplanetary Disk* (Edited by R. H. Hewins, R. H. Jones, and E. R. D. Scott), pp. 257–263.
- BOUWMAN, J., DE KOTER, A., VAN DEN ANCKER, M. E., AND WATERS, L. B. F. M., 2000. The composition of the circumstellar dust around the Herbig Ae stars AB Aur and HD 163296. *A&A* **360**, 213–226.
- BOUWMAN, J., MEEUS, G., DE KOTER, A., HONY, S., DOMINIK, C., AND WATERS, L. B. F. M., 2001. Processing of silicate dust grains in Herbig Ae/Be systems. *A&A* **375**, 950–962.
- BROWNLEE, D. E., 1985. Cosmic dust - Collection and research. *Annual Review of Earth and Planetary Sciences* **13**, 147–173.

- CHOKSHI, A., TIELENS, A. G. G. M., AND HOLLENBACH, D., 1993. Dust Coagulation. *ApJ* **407**, 806–819.
- CUZZI, J. N., HOGAN, R. C., PAQUE, J. M., AND DOBROVOLSKIS, A. R., 2001. Size-selective concentration of chondrules and other small particles in protoplanetary nebula turbulence. *ApJ* **546**, 496–508.
- DOMINIK, C. AND TIELENS, A., 1995. Resistance to rolling in the adhesive contact of two elastic spheres. *Phil. Mag. A* **72**, 783–803.
- DOMINIK, C. AND TIELENS, A., 1996. Resistance to sliding on atomic scales in the adhesive contact of two elastic spheres. *Phil. Mag. A* **73**, 1279–1302.
- DOMINIK, C. AND TIELENS, A., 1997. Coagulation of dust grains and the structure of dust aggregates in space. *ApJ* **480**, 647–673.
- GIBBARD, S. G., LEVY, E. H., AND MORFILL, G. E., 1997. On the possibility of lightning in the protosolar nebula. *Icarus* **130**, 517–533.
- GROSSMAN, J. N., RUBIN, A. E., NAGAHARA, H., AND KING, E. A., 1988. Properties of chondrules. In *Meteorites and the Early Solar System* (Edited by J. F. Kerridge and M. S. Matthews), pp. 619–659, Tucson. The University of Arizona Press.
- HEIM, L.-O., BLUM, J., PREUSS, M., AND BUTT, H.-J., 1999. Adhesion and friction forces between spherical micrometer-sized particles. *Phys. Rev. Lett.* **83-16**, 125–136.
- HORANYI, M. AND GOERTZ, C. K., 1990. Coagulation of dust particles in a plasma. *ApJ* **361**, 155–161.
- JACKSON, J. D., 1975. *Classical Electrodynamics*. John Wiley & Sons, New York, 2nd edn.
- KEMPF, S., 1997. Mikrophysik und Dynamik des Brownschen Staubwachstums in protoplanetaren Scheiben. Ph.D. thesis, Friedr.-Schiller-University Jena.
- KEMPF, S., PFALZNER, S., AND HENNING, T. K., 1999. N-particle-simulations of dust growth. *Icarus* **141**, 388–398.

- KERRIDGE, J. F., 1993. What can meteorites tell us about nebular conditions and processes during planetesimal accretion? *Icarus* **106**, 135+.
- KERRIDGE, J. F. AND MATTHEWS, M. S. (eds.), 1988. Meteorites and the Early Solar System. The University of Arizona Press, Tucson.
- KIVELSON, M. G., BARGATZE, L. F., KHURANA, K. K., SOUTHWOOD, D. J., WALKER, R. J., AND COLEMAN, P. J., 1993. Magnetic field signatures near galileo's closest approach to gaspra. *Science* **261**, 331–334.
- KLAHR, H. H. AND HENNING, T., 1997. Particle-trapping eddies in protoplanetary accretion disks. *Icarus* **128**, 213–229.
- LANDAU, L. D. AND LIFSCHITZ, E. M., 1984. Lehrbuch der theoretischen Physik. Akademie-Verlag, Berlin.
- LEVY, E. H., 1988. Energetics of chondrule formation. In *Meteorites and the Early Solar System* (Edited by J. F. Kerridge and M. S. Matthews), pp. 680–696, Tucson. The University of Arizona Press.
- MALFAIT, K., WAELEKENS, C., WATERS, L. B. F. M., VANDENBUSSCHE, B., HUYGEN, E., AND DE GRAAUW, M. S., 1998. The spectrum of the young star hd 100546 observed with the infrared space observatory. *A&A* **332**, L25–L28.
- MARKIEWICZ, W. J., MIZUNO, H., AND VÖLK, H. J., 1991. Turbulence induced relative velocity between two grains. *A&A* **242**, 286–289.
- MARSHALL, J. AND CUZZI, J., 2001. Electrostatic Enhancement of Coagulation in Protoplanetary Nebulae. In *Lunar and Planetary Institute Conference*, vol. 32, pp. 1262+.
- MEAKIN, P., 1991. Fractal aggregates in geophysics. *Reviews of Geophysics* **29**, 317–354.
- MEAKIN, P. AND DONN, B., 1988. The Effects of Restructuring on the Geometry of Clusters Formed by Diffusion Limited, Ballistic, and Reaction-Limited Cluster-Cluster Aggregation. *ApJ* **329**, L39–L41.
- MIGUEL, M. . AND PASTOR-SATORRAS, R., 1999. Kinetic growth of field-oriented chains in dipolar colloidal solutions. *Phys. Rev. E* **59**, 826–834.



- MIZUNO, H., MARKIEWICZ, W., AND VÖLK, H. J., 1988. Grain Growth in Turbulent Protoplanetary Accretion Disks. *A&A* **195**, 183–192.
- NÜBOLD, H. AND GLASSMEIER, K., 1999. Coagulation and accretion of magnetized dust: A source of remanent cometary magnetism? *Advances in Space Research* **24**, 1167–1173.
- NÜBOLD, H. AND GLASSMEIER, K., 2000. Accretional remanence of magnetized dust in the solar nebula. *Icarus* **144**, 149–159.
- NÜBOLD, H., 1998. Über die Bedeutung magnetisierten Staubs für Aggregationsvorgänge im solaren Urnebel. Master’s thesis, TU Braunschweig.
- NUTH, J. A., 1989. Processes affecting the composition and structure of silicate grains in cometary nuclei. *Earth Moon and Planets* **47**, 33–50.
- NUTH, J. A., FARIS, J., WASILEWSKI, P., AND BERG, O., 1994. Magnetically enhanced coagulation of very small iron grains. *Icarus* **107**, 155+.
- NUTH, J. A. AND WILKINSON, G. M., 1995. Magnetically enhanced coagulation of very small iron grains: A correction of the enhancement factor due to dipole-dipole interactions. *Icarus* **117**, 431–434.
- OSSENKOPF, V., 1993. Dust coagulation in dense molecular clouds: the formation of fluffy aggregates. *A&A* **280**, 617–646.
- POPPE, T., BLUM, J., AND HENNING, T., 2000. Analogous experiments on the stickiness of micron-sized preplanetary dust. *ApJ* **533**, 454–471.
- RAPAPORT, D. C., 1995. The Art of Molecular Dynamics Simulation. Cambridge University Press, Cambridge.
- RICHARDSON, D. C., 1995. A self-consistent numerical treatment of fractal aggregate dynamics. *Icarus* **115**, 320–335.
- RICHTER, I. E. A., 2001. First direct magnetic field measurements of an asteroidal magnetic field: Ds1 at braille. *Geophys. Res. Lett.* in press.
- RIETMEIJER, F. J. M., NUTH, J. A., AND KARNER, J. M., 1999. Metastable eutectic condensation in a Mg-Fe-SiO-H<sub>2</sub>O<sub>2</sub> vapor: Analogs to circumstellar dust. *ApJ* **527**, 395–404.

- SCHULZE, H., KISSEL, J., AND JESSBERGER, E. K., 1997. Chemistry and mineralogy of halley’s dust. In *From Stardust to Planetesimals* (Edited by Y. J. Pendleton, A. G. G. M. Tielens, and M. L. Savage), vol. 122 of *ASP Conference Series*, p. 397.
- STREETT, W. B., TILDESLEY, D. J., AND SAVILLE, G., 1977. Multiple time-step methods in molecular dynamics. *Molecular Phys* **35**, 639–648.
- SUGIURA, N. AND STRANGWAY, D. W., 1988. Magnetic studies of meteorites. In *Meteorites and the Early Solar System* (Edited by J. F. Kerridge and M. S. Matthews), pp. 595–618, Tucson. The University of Arizona Press.
- WATERS, L. B. F. M. AND WAELEKENS, C., 1998. Herbig Ae/Be stars. *Ann. Rev. Astro. Astrophys.* **36**, 233–266.
- WEIDENSCHILLING, S. J., 1977. Aerodynamics of solid bodies in the solar nebula. *MNRAS* **180**, 57–70.
- WEIDENSCHILLING, S. J., 1980. Dust to planetesimals - settling and coagulation in the solar nebula. *Icarus* **44**, 172–189.
- WEIDENSCHILLING, S. J., 1984. Evolution of Grains in a Turbulent Solar Nebula. *Icarus* **60**, 553–567.
- WEIDENSCHILLING, S. J., 1997. When the dust settles - Fractal aggregates and planetesimal formation. In *Lunar and Planetary Science Conference*, vol. 28, pp. 1517+.
- WEIDENSCHILLING, S. J. AND CUZZI, J. N., 1993. Formation of planetesimals in the solar nebula. In *Protostars and Planets III* (Edited by E. H. Levy and J. I. Lunine), Tucson. University of Arizona Press.
- WEIDENSCHILLING, S. J., DONN, B., AND MEAKIN, P., 1988. The Physics of Planetesimal Formation. In *The Formation and Evolution of Planetary Systems* (Edited by H. A. Weaver and L. Danly), pp. 131–150, Cambridge, New York, Melbourne, Sydney. Cambridge University Press.
- WEIDENSCHILLING, S. J. AND RUZMAIKINA, T. V., 1994. Coagulation of Grains in Static and Collapsing Protostellar Clouds. *ApJ* **430**, 713.

- WHITTAKER, E. T., 1904. A treatise on the analytical dynamics of particles and rigid bodies. Cambridge University Press.
- WITHEY, P. A. AND NUTH, J. A., 1999. Formation of Single-Magnetic-Domain Iron Particles via Vapor-Phase Nucleation: Implications for the Solar Nebula. *Icarus* **139**, 367–373.
- WURM, G., 1997. Experimentelle Untersuchungen zu Bewegung und Agglomerationsverhalten mikrometergroßer Teilchen in protoplanetaren Scheiben. Ph.D. thesis, Friedr.-Schiller-University Jena.
- WURM, G. AND BLUM, J., 1998. Experiments on preplanetary dust aggregation. *Icarus* **132**, 125–136.

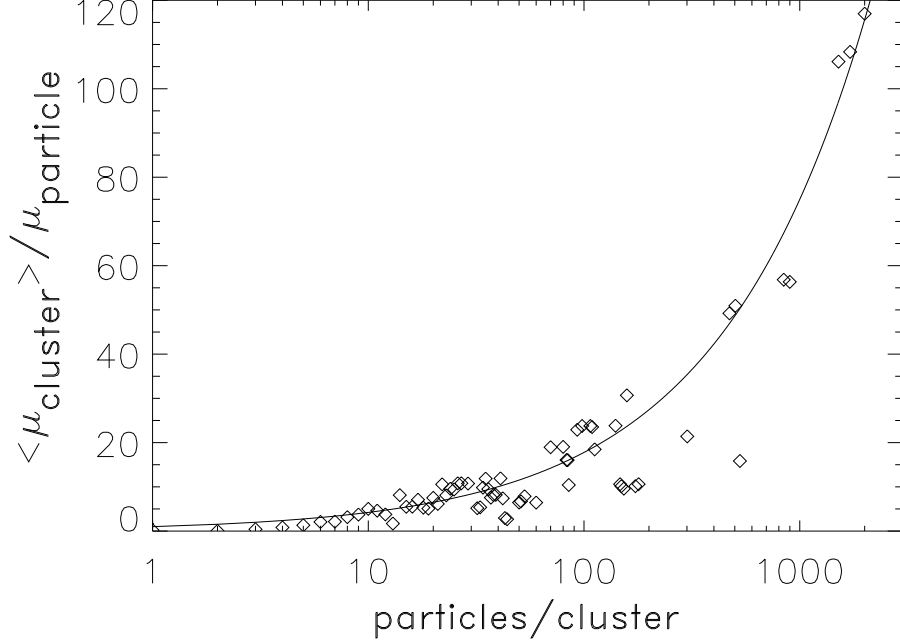


FIG. 1. *Accretional remanence*: The increase of cluster magnetic moment with the number of individual magnetic grains in numerical simulations (NÜBOLD AND GLASSMEIER, 1999, 2000). The curve illustrates the relationship  $\mu \propto N^{0.63}$ , which shows the strong tendency of magnetized grains to acquire a state of minimum magnetostatic energy (cf. Eq. 7), i.e. a pole-to-pole configuration for each pair of grains, and the misalignment effect caused by thermal agitation as well as the microphysics of the coagulation process.

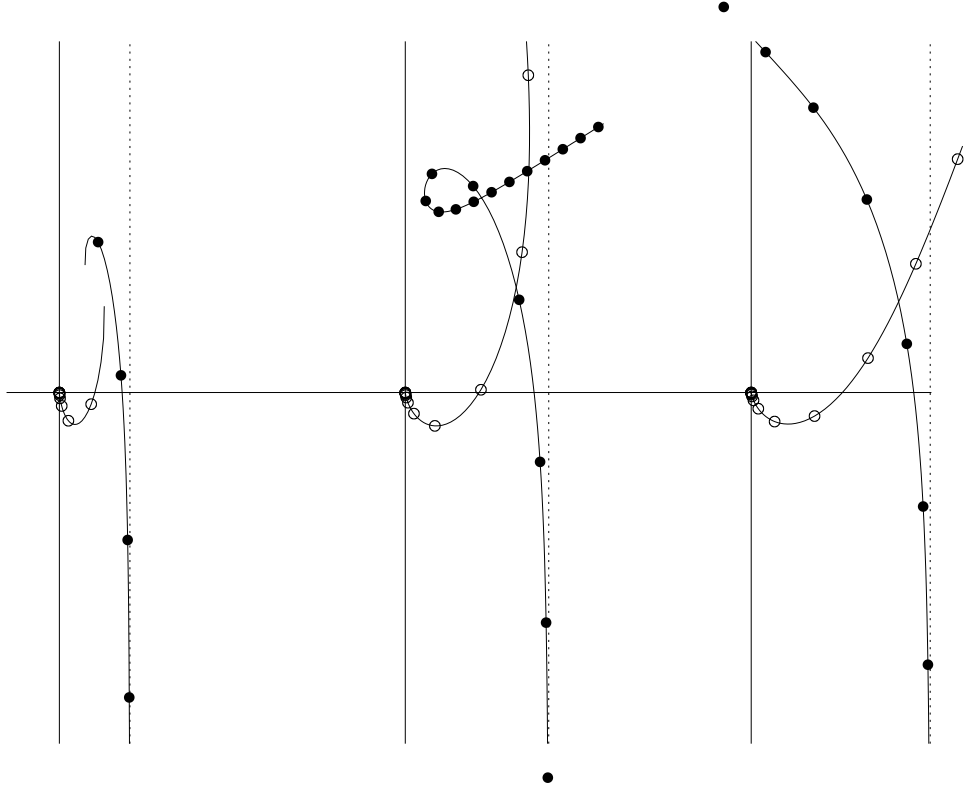


FIG. 2. Three example trajectories of numerical collision experiments with *SAND*. The particles are 20 nm iron grains with a magnetic moment of  $200 \text{ Am}^2\text{kg}^{-1}$  and thermal rotations derived from a Maxwellian distribution at 100 K. Initial velocity is  $v_{\text{th}}/16$ . The impact parameters are 0.95, 1.0, and 1.025 times the analytically derived maximum impact parameter  $b_{\text{max}}$ , respectively. Note that the size of the dots does not indicate the size of the grains which would be hardly visible on this scale since  $b_{\text{max}} \approx 250R$ .

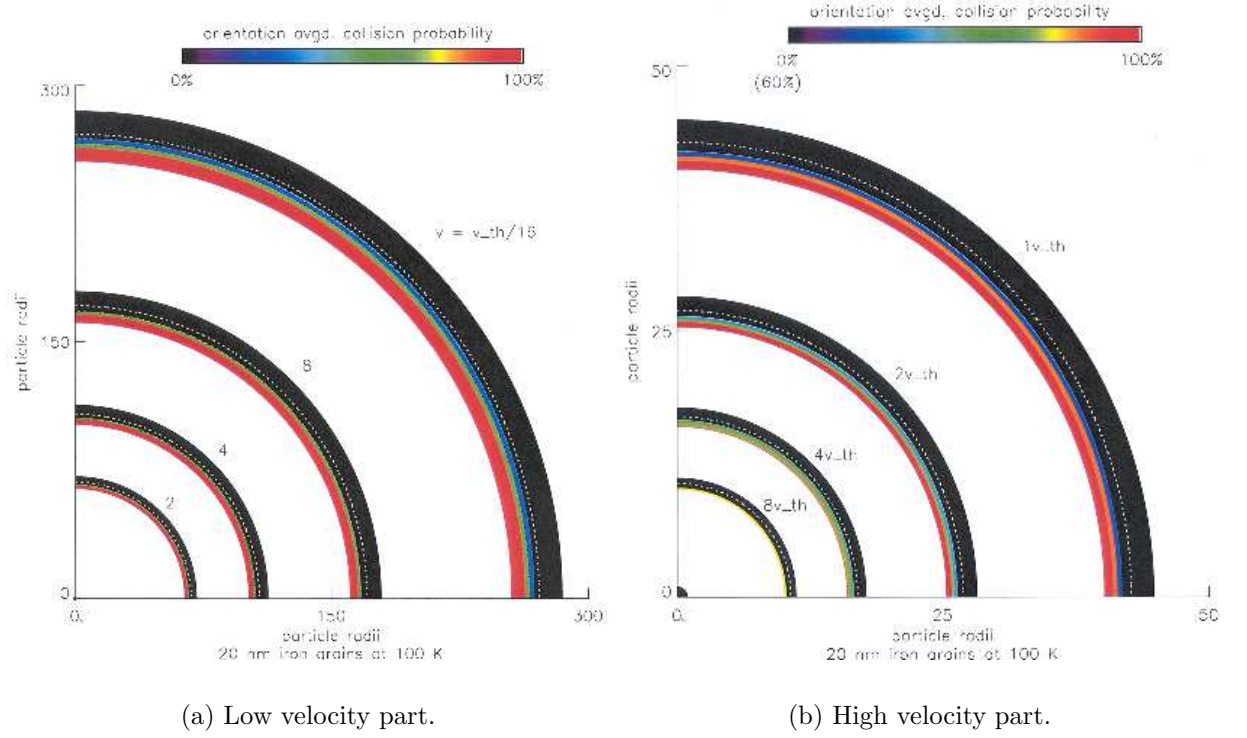


FIG. 3. Numerical validation of Eq. 14. Collision probabilities for different relative velocities and impact parameters are orientation averaged and color-coded. *Black* means that for no relative orientations of dipoles a collision could be detected. *White* means that all randomly chosen orientations resulted in a collision. For one specific velocity, all the area *outside* the black annular region should be black as well, the same holds for the area *inside* the white annular region, which should be all white. Please note that the color bar has been compressed for the high velocity regime, with black coding meaning  $p \leq 60\%$ . The dashed lines denote the theoretically derived cross section according to Eq. 14.

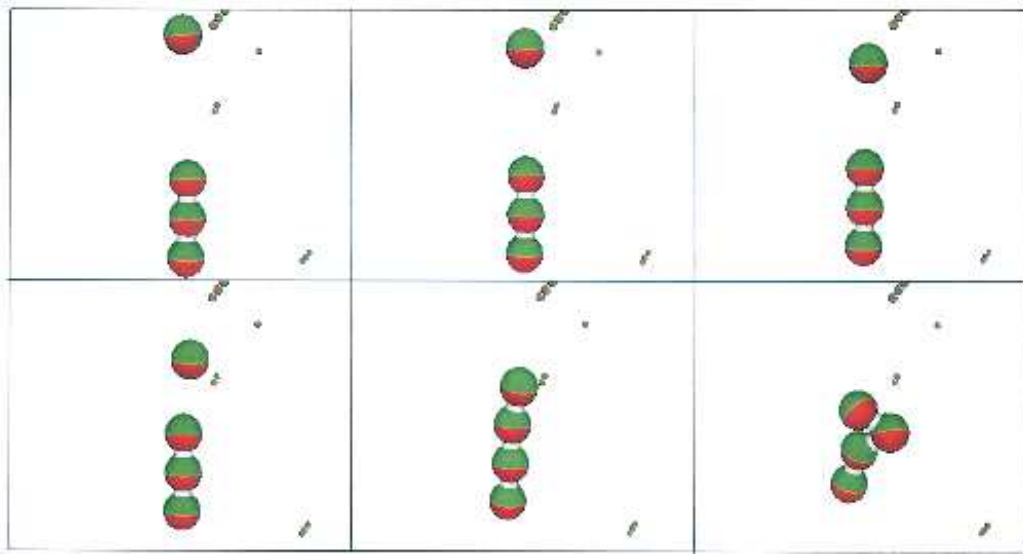


FIG. 4. Example of a collision between a chain and a single particle which illustrates that the detailed treatment of contact forces is important to determine the correct structure of an aggregate. The impact of the incoming grain moves the grain at the end of the chain. The resulting T-like structure would not have resulted from a simple hit-and-stick approximation.

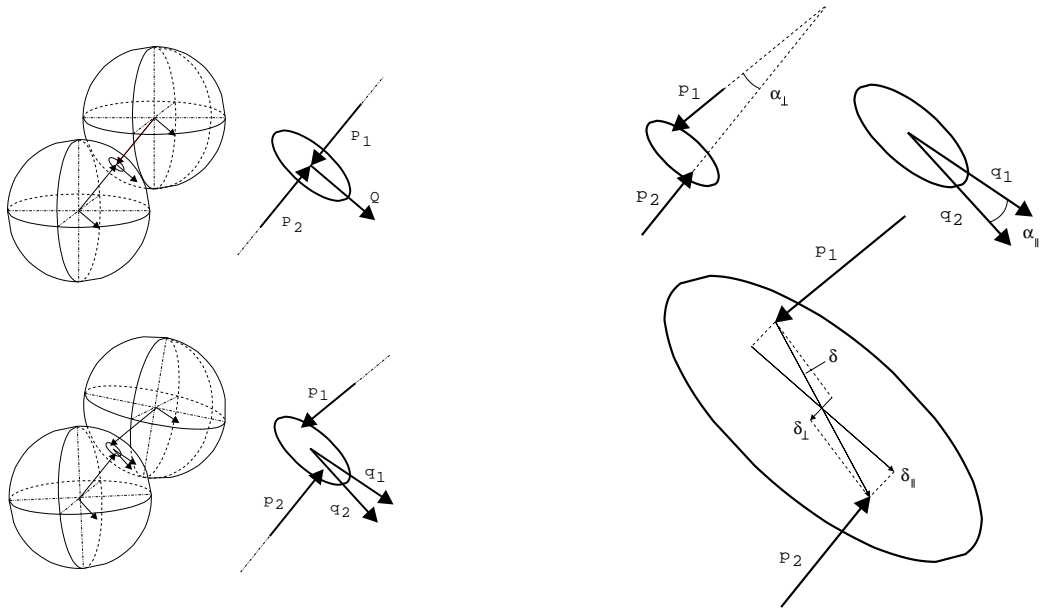


FIG. 5. Geometrical treatment of contact displacements. Left panel: Contact between two grains in equilibrium (top) and in stressed configuration (bottom). Right panel: Blow-up of the contact region with definitions of the displacement vectors. See text.